

Hess-2014-409 Understanding NMR relaxometry of partially water-saturated rocks

O.M. Mohnke, C.N. Nordlund, R.J. Jorand, and N.K. Klitzsch

Handling Editor: Prof Mauro Giudici, mauro.giudici@unimi.it

Manuscript Type: Research Article

**Response to editor / reviewers**

Dear Prof. Giudici and reviewers,

Thank you for your additional comments and corrections. We have corrected and revised the manuscript in accordance to your suggestions and also re-checked consistency of the used units, symbols used in the text and figures.

Our responses to the specific comments are attached in a separate document along with the revised manuscript and track-change document. I am looking forward to hearing from you.

Kind regards,

Oliver Mohnke

Hydrol. Earth Syst. Sci. Discuss., 11, C5692–C5694, 2014  
www.hydrol-earth-syst-sci-discuss.net/11/C5692/2014/  
© Author(s) 2014. This work is distributed under  
the Creative Commons Attribute 3.0 License.

Hydrology and  
Earth System  
Sciences

Open Access

Discussions

**Interactive comment on “Understanding NMR relaxometry of partially water-saturated rocks”**

**by O. Mohnke et al.**

Received and published: 15 December 2014

**Responses to specific reviewer comments**

**Anonymous Referee #1**

**General**

Figure 2b) With regard to the initial condition, where does the shift to slower relaxation times (96-89) in the beginning comes from?

We checked the data and discovered an error in our data plot processing, mixing up data entries from different samples of the study. We exchanged figure 2b with the correct T1 distribution results.

Figure 8, 9 and 11.

Where does the difference in the surface relaxivity parameter  $10^{-5}$  m/s to  $10^{-10}$  m/s comes from?

No difference, corrected the typo in units m vs us

Page 12698

Line 4 the NMR signal amplitude needs to be extrapolated to be proportional to porosity  
Changed to ‘initial signal amplitude’

Line 5-7 state that “[. . .] the relationship between pore size and NMR relaxation depends on pore shape [. . .]” whereas in the conclusions on page 12712 line 12 -14 “The NMR relaxation time depends on the surface-to-volume ratio (not on pore shape) [. . .]” is written. Please clarify, this seems contradictory.

We agree, and clarified this statement, to avoid confusion between NMR behavior at fully and partially saturation

Page 12705

Line 6 The whole paragraph needs to be more clear since the loss of phase coherence is a T2 issue and therefore not related to T1 as Eq. 8 states.

Clarified and removed reference to T2 phase coherence effects

## Technical

Figures should be larger and printed in high resolution, they are hard to read in terms of font size and color

Figures image files are basically all in a good resolution, but seemingly were degraded during pdf conversion. We will possibly need check on that with HESS layouter

Figure 8b and c) decay time? T1 or T2?

Figure 10) decay time? T1 or T2?

Added 'longitudinal' magnetization in the respective captions in Fig 8, 9 and 10 to clarify (it is already referred to the NMR relaxation as T1)

Figure 8. Surface relaxivity has a wrong unit

Corrected

Figure 14) decay time? T1 or T2?

Corrected the plots to show T1 buildup signal behavior and corrected and clarified the caption

Figure 14. Amplitude of what? T1 or T2? Is this the extrapolated amplitude?

Clarified, that it is related to T1; Note, as we show simulated data we can directly calculate initial amplitude  $M_0(t=0)$  similar to measured NMR data the integral of inverted T1 distributions yields the initial amplitude.

Page 12698

Line 25 delete "the"

Corrected

Page 12699

Line 6-9 the extrapolated signal amplitudes are proportional

Changed to 'initial signal amplitudes'

Page 12700

Line 22 insert blank between "and water"

Corrected

Page 12701

Line 25 air is not a fluid, I suggest to use the phrase "non-wetting phase" instead of Fluid

Changed to "non-wetting phase" (also changed the other occurrence on page12702, L2)

Page 12705

Line 11 I assume that you mean that the [ . . ]molecules diffuse at the wall [ . . ]- please clarify

Changed to "diffuse to at the pore walls"

## S. Costabel (Referee)

stephan.costabel@bgr.de

General comments:

The manuscript suggests the use of capillaries with triangular cross-sections for interpreting NMR relaxometry data of partially saturated rocks. Using this kind of pores, one accounts for remaining water menisci during de-saturation trapped by capillary forces in the corners of the triangle. After explaining the known properties of such pore systems regarding drainage/imbibition and the physical relationship between pore pressure and remaining water content, the NMR response of the water menisci is analytically derived and verified by numerical simulations. The NMR properties of single capillaries with triangular cross-section as well as a corresponding bundle of capillaries (pore size distribution) are analyzed and compared to usual circular capillaries. Unfortunately, the authors show only one real NMR data example (Rotliegend sandstone) to motivate the necessity of their study. Therefore, I am afraid that the relevance of this paper might be questioned by the community. However, I know from own experience with loose sediments that the phenomenon of occurring relaxation regimes for  $S < 1$  outside the original relaxation time distribution at  $S = 1$  can very often be observed, even with pure sand. I urgently suggest to show more own data or refer to literature with further data examples for motivation (e.g. Costabel, 2011; Bird et al., 2005; Jäger et al. 2009).

**We added additional references (also, see comments below)**

I suggest to accept the paper after major revisions.

The step from single pore to pore size distribution must be explained, analyzed and discussed more in detail. I would be glad to see a figure similar to Fig. 1 (de-saturation for the bundle of circular capillaries) also for the distribution of triangles.

**Included figure with desaturated triangular pore size distributions and added discussion in text**

Furthermore, the critical role of hysteresis and its representation in the simulated NMR data is not worked out adequately, although the authors mention this in the Summary/Conclusions section as key feature of their approach (P 12711 L 17).

**We added additional figures and included a paragraph to better illustrate and clarify the observed hysteresis behavior.**

I doubt that hysteresis effects can be observed unambiguously using NMR relaxometry.

**Agreed, possibly a very challenging experiment to demonstrate. Other complementary data, a priori information/assumptions and/or model constraints would be required. However, the main focus here is on introducing and promoting a basic model towards improving the understanding of NMR behavior on partially saturated rocks or soil.**

However, I believe that the key feature of triangular pore spaces is the exact description of the physical relationship between remaining water content, pore pressure and permeability/hydraulic conductivity (e.g. Tuller and Or, 2001).

Using this relationship for interpreting NMR data would be a clear benefit and this manuscript has the potential to show the way how this can be done.

Best regards, Stephan Costabel

Additional references:

Costabel, S.: Nuclear magnetic resonance on laboratory and in field scale for estimating hydraulic parameters in the vadose zone, PhD thesis, Berlin University of Technology, 2011. ([opus4.kobv.de/opus4-tuberlin/files/3173/costabel\\_stephan.pdf](http://opus4.kobv.de/opus4-tuberlin/files/3173/costabel_stephan.pdf))

Added above reference and additional comments regarding in the text (see below)

Bird, N. R. A., Preston, A. R., Randall, E. W., Whalley, W. R., and Whitmore, A. P. (2005). Measurement of the size distribution of water-filled pores at different matric potentials by steady state nuclear magnetic resonance. *European Journal of Soil Science*, 56:135143.

Jaeger, F., Bowe, S., van As, H., and Schaumann, G. E. (2009). Evaluation of  $^1\text{H}$  NMR relaxometry for the assessment of pore size distribution in soil samples. *European Journal of Soil Science*, 60:1052 – 1064.

Added above references

Specific comments:

P 12699 L 20: Include (2006) after citing Al-Mahrooqi et al.  
corrected

P 12700 L 22: Include a space after “and”  
corrected

P 12700 L 26: Costabel (2011) analytically derived the NMR response of a single water meniscus for the first time (for an arbitrary opening angle and for the fast diffusion regime, Costabel, 2011, Pages 33 – 38). It would be fair to cite this work, even if it is (only?!) a part of the PhD thesis and not published as a peer reviewed paper. Costabel (2011) analyzed the relationship between mean relaxation time (= single angular pore system) and saturation degree (Costabel, 2011, Pages 33 – 41). He also concluded that, when considering capillaries with angular cross-sections, new relaxation regimes will occur during de-saturation that might exceed the relaxation time distribution at  $S=1$  towards smaller relaxation times (Costabel, 2011, Page 61).

Agreed, this goes without any questions! We have cited this work accordingly.

P 12701 L 2: I could not figure out what you mean by “. . . the simulated signals are tested using synthetic pore size distributions.” Do you really test the simulated signals? As I understand, you simulate signals based on synthetic pore size distributions.

We clarified the sentence

P 12701 L 20: “. . . gravity forces are weak.” Actually, these are neglected.

### Added comments in the text

P 12705 L 11 - 14: I suggest to include the term “fast diffusion” anywhere in this sentence.

P 12708 L 4: The term “fast diffusion” is referred to here for the first time without any further explanation. Please introduce it first (e.g. at P 12705 L 11-14).

C5735

Introduced fast diffusion term in 12705, L11ff

P 12709 L5: Fig.11 has no subplot “a”.

Deleted the reference to Fig.11a

P 12709 L9: Include “partially saturated” before “system of pores”

Corrected

P 12709 L 18 to P 12710 L 7: I do not understand the necessity of combining the analyses of the drainage/imbibition behavior of the angular pore system and the NMR response of that system in this passage. The focus jumps from Fig. 14 to Fig. 13, then back to 14 and back again to 13, before Fig. 14 is analyzed in detail, which is quite confusing. Finally, no effects of hysteresis can be observed in the simulated NMR data in Fig.14. Indeed, I would not expect that any drainage/imbibition behavior can be made visible using these NMR simulations. Therefore, I suggest to compare and discuss the hysteresis effects of the pore systems earlier, e.g. after introducing the de-saturation behavior of the single pores in Fig. 4 and Fig. 5. Here, in section 2.3 you should focus the discussion on the NMR responses at partial saturation only. If you do not agree, please explain more in detail how the hysteresis effects influence the NMR data and discuss how this influence can possibly be used in future interpretation schemes. I expect that there is a natural ambiguity between drainage and imbibition that cannot be resolved by NMR relaxometry.

We added additional figures and rearranged paragraphs so for a more consistent read without jumping to better address these items (also, see our response above)

P 12710 L 8 ff: In addition to my concerns above, some important details on the simulations in Fig.14 are missing. What are the properties of the underlying pore size distributions for the three cases?

What are the values for  $T_{\text{bulk}}$  and surface relaxivity.

Why did you choose the T2 relaxation here in contrast to the T1 simulations in Fig. 8 and 9? Possibly, this information should be introduced together with Fig.12, but Fig.12 is not mentioned in the text at all. Seems to be a lognormal distribution: what are the values for the mean and the standard deviation?

Parameters for pore size distribution were included and changed the figures to be consistent with the previous discussion of NMR T1 relaxation. Also, the order of figures was adjusted accordingly.

P 12710 L 25: Regarding the assumption of pore size distributions based on triangular capillaries, there is a principle problem occurring during de-saturation. The pore system is considered to be a bundle of triangular capillaries and each capillary has its individual size, but all are similar in shape. After the snap-off, the contribution of each capillary to the NMR relaxation behavior is identical, even if they are originally different

in size. This is because the de-saturation is controlled by the pressure, which determines the curvature of the arc meniscus. Following the concept of reduced geometry all de-saturated triangles with their remaining water in the corners look the same. Consequently, at some point during de-saturation, i.e., if the air has entered all capillaries of the pore system, only one single relaxation time is left for the case of the equilateral triangles (Fig. 14b) or three relaxation times for the case of the right-angled triangles (Fig. 14c). Strictly speaking, the assumption of a relaxation time distribution is no longer valid at this point. This is a conceptual problem and must be discussed at the end of this section.

Agreed, we are aware of this inherent behavior of a single (or n) corner related discrete decay times. Seemingly, becoming somewhat 'professionally blinkered' of this 'obvious' behavior we did not include this particular point in our initial discussion. We have thankfully taken up on that comment and added a figure and discussion of this behaviour.

This feature is of course not captured in the typical inverse modeling approach for NMR lab/log data we used here. We also tried to address this accordingly in discussion and conclusion It is intended to implementing this concept an adapted future inversion scheme mentioned as part of our outlook.

P 12711 L 17 – 19: A discussion is missing on how the hysteresis behavior is encoded in the NMR data. This is not obvious from Fig. 14. Please see also my comment on P 12709 L 18 to P 12710 L 7.

Include NMR related hysteresis plots in a consolidated figure (Fig. 15)

P 12711 L 12: On the statement “. . .triangular pores strongly influence . . . hydraulic properties”. Tuller and Or (2001) derived the hydraulic conductivities for different crossections of capillaries, also for the equilateral triangle. What relationship between shape/size of the triangle and saturated hydraulic conductivity must be expected? Such information would strengthen your statement a lot.

We added a paragraph and discussed this relationship

P 12711 L 22 - 25: You should explain in detail what benefits are expected of such an inversion scheme compared to the classical approach of using circular capillaries. What are the shortcomings of existing approaches for partial saturation if the remaining water menisci remain unconsidered?

We tried to point out and list possible benefits, e.g. NMR inversion on partially saturated rocks when estimating surface relaxivity or predicting relative permeability from laboratory or borehole data

# 1 Understanding NMR relaxometry of partially water-saturated rocks

2 O. Mohnke, R. Jorand, C. Nordlund, N. Klitzsch

3 Institute for Applied Geophysics and Geothermal Energy (GGE), E.ON Energy Research

4 Center (E.ON ERC), RWTH Aachen University, Mathieustrasse 10, 52074 Aachen

5

## 6 Abstract

7 Nuclear Magnetic Resonance (NMR) relaxometry measurements are commonly used to  
8 characterize the storage and transport properties of water-saturated rocks. ~~These assessments~~  
9 ~~Estimations of these properties~~ are based on the ~~proportionality-direct link~~ of ~~the initial~~ NMR  
10 ~~initial-signal amplitude to porosity (water content)~~ and ~~of the NMR~~ relaxation times ~~to~~  
11 ~~porosity (water content) and to~~ pore size, ~~respectively~~. Herein, pore shapes are usually  
12 assumed to be spherical or cylindrical. However, the NMR response at partial water  
13 saturation for natural sediments and rocks may differ strongly from the responses calculated  
14 for spherical or cylindrical pores, because these pore shapes ~~cannot-do not~~ account for water  
15 menisci remaining in the corners of de-saturated angular pores. Therefore, we consider a  
16 bundle of pores with triangular cross-sections. We introduce analytical solutions of the NMR  
17 equations at partial saturation of these pores, which account for water menisci of de-saturated  
18 pores. After developing equations that describe the water distribution inside the pores, we  
19 calculate the NMR response at partial saturation for imbibition and drainage based on the  
20 deduced water distributions.

21 For this pore model, ~~the~~ NMR amplitudes and NMR relaxation times at partial water  
22 saturation strongly depend on pore shape, ~~i.e., arising from the capillary pressure and pore~~  
23 ~~shape dependent water distribution in desaturated pores with triangular cross-sections.~~ ~~even~~  
24 ~~Even so,~~ the NMR relaxation time at full saturation only depends on the ~~surface-surface-to-to-~~  
25 volume ratio of the pore. ~~The pore-shape-dependence at partial saturation arises from the pore~~



26 | ~~shape and capillary pressure dependent water distribution in pores with triangular cross-~~  
27 | ~~sections.~~ Moreover, we show the qualitative agreement of the saturation dependent relaxation  
28 | time distributions of our model with those observed for rocks and soils.

## 29 **1 Introduction**

30 Understanding multi-phase flow processes in porous rocks and soils is vital for addressing  
31 a number of problems in geosciences such as oil and gas recovery or vadose zone processes,  
32 which influence groundwater recharge and evaporation. Effective permeability, which is  
33 defined as the permeability of a fluid in the presence of another fluid, is the decisive  
34 parameter for fluid transport, and depends on fluid saturation, wetting condition, and pore  
35 structure. In addition, saturation history influences the fluid content and the effective  
36 permeability (for a specific pressure), which are different for imbibition and drainage.

37 A method considered suitable for determining water content of rocks non-invasively is  
38 nuclear magnetic resonance (NMR), because the NMR initial signal amplitudes are directly  
39 proportional to the hydrogen content in the pore space, and the NMR relaxation times are  
40 linked to the size of the water-containing pores in the rock. In a two-phase system of water  
41 and air only the water contributes to the NMR signal response. Therefore, NMR is widely  
42 used for estimating transport and storage properties of rocks and sediments (Kenyon, 1997;  
43 Seevers 1966; Fleury et al., 2001; Arnold et al., 2006).

44 In recent years, several researchers have studied the relationship between NMR and  
45 multiphase flow behavior on the pore scale to better understand and infer the storage and  
46 transport properties of partially saturated rocks or sediments (e.g., Chen et al., 1994; Liaw et  
47 al. 1996; Ioannidis et al., 2006; Jia et al., 2007; Al-Mahrooqi et al., 2006; Costabel and  
48 Yaramanci, 2011, 2013; Talabi et al., 2009). As an extension of this research, we study the  
49 relationship between the water distribution inside the pores of a partially saturated rock and  
50 the system's NMR response by using bundles of pore with triangular cross-sections. While  
51 Al-Mahrooqi et al. (2006) used a similar modeling approach to infer the wettability properties  
52 in oil-water systems, this study investigates the evolution of the NMR relaxation-time spectra  
53 during drainage and imbibition. For this purpose, we consider a capillary pore ensemble that

54 is partially saturated with water and air. Traditionally, the pores within this ensemble are  
55 assumed to have a cylindrical geometry. Depending on pressure, cylindrical capillaries are  
56 either water- or air-filled and thus they either contribute to an NMR response or ~~they do not~~.  
57 Consequently, the NMR relaxation times of partially water-saturated capillary pore bundles  
58 always remain subsets of the fully saturated system's relaxation-time distribution, i.e., they  
59 are a function inside the envelope of the distribution curve at full saturation (see Fig. 1).  
60 However, in porous rocks, which are formed by the aggregation of grains, the pore geometry  
61 is usually more complex (Lenormand et al., 1983; Ransohoff and Radke, 1987; Dong and  
62 Chatzis, 1995) and may exhibit angular and slit-shaped pore cross-sections rather than  
63 cylindrical capillaries or spheres (Fig. 2a). For example, in tight gas reservoir rocks Desbois  
64 et al. (2011) found three types of pore shapes that are controlled by the organization of clay  
65 sheet aggregates: i) elongated or slit-shaped, ii) triangular, and iii) multi-angular cross-  
66 sections. The relaxation-time distribution functions derived from NMR measurements for  
67 such partially saturated rocks are frequently found to be shifted towards shorter relaxation  
68 times outside the original envelope observed for a fully saturated sample, (Fig. 2b) (e.g.,  
69 Applied Reservoir Technology Ltd., 1996; Bird, et al., 2005; ~~;-Jaeger et al., 2009; Jorand et~~  
70 ~~al., 2010; -Stingaciu, 2010a,b; Costabel, 2011).~~  
71 In angular pores, water will remain trapped inside the pore corners even if the gas entry  
72 pressure is exceeded. Standard NMR pore models that assume cylindrical or spherical pore-  
73 ensembles (e.g., Kenyon, 1997), however, do not account for such residual water (~~Blunt et~~  
74 ~~al., 2002; Tuller et al., 1999; Or and Tuller, 2000; Tuller and Or, 2001; Thern, 2014).~~ To  
75 overcome this limitation, we adopt a NMR modeling approach initially proposed and  
76 discussed by Costabel (2011) and present numerical simulations and analytical solutions of  
77 the NMR equations for partially saturated pores with triangular cross-sections to quantify  
78 NMR signal amplitudes and relaxation times. The NMR response of a triangular capillary

79 during drainage and imbibition depends on the water distribution inside the capillary, which  
80 is subject to pore shape and capillary pressure. Thus, in the next chapter we present the  
81 relationship between capillary pressure and water distribution inside cylindrical and  
82 triangular pore geometries during drainage and imbibition. For this purpose, the reduced  
83 similar geometry concept introduced by Mason and Marrow (1991) is used. Subsequently,  
84 based on the spatial water distribution, an analytical solution of the NMR diffusion equation  
85 (Torrey, 1956; Brownstein and Tarr, 1979) for partially saturated triangular capillaries is  
86 derived and tested by numerical simulations (Mohnke and Klitzsch, 2010). The derived  
87 equations are used to study the influence of pore size distribution and pore shape of triangular  
88 capillaries on the NMR response, in particular considering the effects of trapped water.  
89 Finally, an approach for simulating NMR signals during imbibition and drainage of triangular  
90 pore capillaries is introduced and demonstrated using synthetic pore size distributions.

91

## 92 **2 Results and discussion**

### 93 **2.1 Water distribution during drainage and imbibition in a partially saturated** 94 **triangular tube**

95 In a partially saturated pore space, a curved liquid-vapor interface called the arc meniscus  
96 (AM) arises due to the pore's capillary forces. In addition, adsorptive forces between water  
97 and matrix lead to the formation of a thin water film at the rock-air interface. Such water  
98 films with a thickness typically below 20 nm (e.g., Toledo et al., 1990; Tokunaga and Wan,  
99 1997) exhibit very short NMR relaxation times. Although water films to some extent may  
100 influence transport properties and water distribution of a partially saturated porous system  
101 (Tuller and Or, 2001), the contribution of the film volume to NMR amplitudes is very small  
102 with respect to the NMR signal amplitudes arising from the water trapped in the menisci, i.e.,  
103  $V_{\text{film}} \ll V_{\text{meniscus}}$ . Therefore, for sake of simplicity, we neglect water films in his study.

104 In the following discussion, we consider a triangular capillary, initially filled with a  
 105 perfectly wetting liquid, i.e., contact angle  $\theta = 0^\circ$ , which exhibits a constant interfacial  
 106 tension  $\sigma$  ( $\sigma_{\text{air-water}} = 73 \times 10^{-3} \text{ Nm}^{-1}$  at  $20^\circ\text{C}$ ) and is under the assumption that gravity  
 107 forces are weak and therefore can be neglected. The two-phase capillary entry pressure as  
 108 derived by the MS-P method (Mayer and Stowe, 1965; Princen, 1969a, b, 1970) can be  
 109 expressed by the Young-Laplace equation:

$$p_c = \frac{\sigma \cos \theta}{r_{\text{AM}}} = \frac{\sigma}{r_{\text{AM}}}, \quad (1)$$

110 where  $r_{\text{AM}}$  is the radius of the interface arc meniscus and  $p_c$  is the minimum pressure  
 111 difference necessary for a non-wetting phase, i.e., air, to invade a uniformly wetted (tri-)  
 112 angular tube filled with a denser phase, i.e., water (see Fig. 3a). Upon consideration of a  
 113 pressure difference  $p > p_c$ , the non-wetting phase will begin to enter the pore and occupy the  
 114 central portion of the triangle, whereas – separated by the three interface arc menisci of radius  
 115  $r_{\text{AM}}$  – the wetting fluid remains in the pore corners (Fig. 3a).

116 From an original triangle  $ABC$ , a new smaller triangle  $A'B'C'$  of similar geometry with an  
 117 inscribed circle of radius  $r' = r_{\text{AM}} < R_0$  can be constructed by means of the reduced similar  
 118 geometry concept as introduced by Mason and Morrow (1991) (Fig. 3b). To account for  
 119 different transport mechanisms during imbibition and drainage of the denser wetting phase,  
 120 Mason and Morrow (1991) introduced two different principal displacement curvatures with  
 121 radii  $r_I$  and  $r_D$ , respectively.

122 During imbibition of a (tri-)angular pore, the radius of curvature  $r_{\text{AM}}$  increases until the  
 123 separate arc menisci of the corners touch and the pore fills spontaneously (“snap off”). The  
 124 critical radius of curvature  $r_I$ , which is equal to the radius of the pore’s inscribing circle, for  
 125 the angular pore at “snap-off” pressure  $p_I$  is then given by

$$r_I = \frac{2A}{p}, \quad (2)$$

126

127 According to Eq. 2, the snap-off pressure depends on the geometry of the triangle only,  
128 i.e., on its cross-sectional area  $A$  and perimeter  $P$ . In contrast, during drainage the threshold  
129 radius of curvature  $r_D = r_{AM}$ , at which the center of the fully saturated angular capillary  
130 spontaneously empties as ~~a~~the non-wetting fluid phase invades the pore, is given by

$$r_D = P \left[ \frac{1}{2G} + \left( \frac{\pi}{G} \right)^{1/2} \right]^{-1}, \quad (3)$$

131 with  $r_D < r_I$  and drainage threshold pressure  $p_D > p_I$ . The dimensionless and size-  
132 independent factor  $G = \frac{A}{P^2} \left( = \frac{A'}{P'^2} \right)$  reflects the shape of the triangle depending on its cross-  
133 sectional area  $A$  and perimeter  $P$  ( $A'$  and  $P'$  refer to the reduced triangle), i.e., from near-slit-  
134 shape ( $\lim_{\gamma \rightarrow 0} G = 0$ ) to equilateral shape ( $G = 0.048$ ). A detailed derivation of Eqs. 2 and 3  
135 as a consequence of hysteresis between drainage and imbibition can be found in Mason and  
136 Morrow (1991).

137 ~~Note, that the~~The permeability of a porous system of such triangular capillaries is  
138 strongly influenced by the shape factor  $G$ . For single-phase laminar flow in a triangular tube  
139 the hydraulic conductance  $g$  is given by the Hagen-Poiseuille formula

$$g = k \frac{A^2 G}{\mu} \quad (4)$$

140 with the cross-sectional area  $A$ , the shape factor  $G$ , the fluid viscosity  $\mu$ , and  $k$  being a  
141 constant accounting for the geometrical shape of the cross-section, e.g.  $k = 0.5$  for circular  
142 tubes and  $k = 0.6$  for a tube with a cross-section of an equilateral triangle (Patzek and Silin,  
143 2001). The hydraulic conductance of an irregular triangle is closely approximated by  
144 equation 1 using the same constant  $k$  as for an equilateral triangle (Øren et al., 1998). Thus,

145 for a constant cross-sectional area the hydraulic conductance  $g$  of the pore is proportional to  
 146 its shape factor  $G$ .

147 Combining Eqs. 1–3 with the concept of reduced similar geometry discussed above, the  
 148 degree of water saturation ( $S_w$ ) inside a single triangular tube with cross-sectional area  $A_0$ ,  
 149 perimeter  $P_0$ , and radius  $R_0$  of its inscribing circle at a given capillary pressure  $p_c$  during  
 150 imbibition and drainage can be calculated according to

151

$$S_w^I(p, A_0, P_0) = \begin{cases} 1 & , p_c \leq p_I \quad (R_0 \leq r_I) \\ \frac{A_\Delta(p_c)}{A_0} & , p_c > p_I \quad (R_0 > r_I) \end{cases} \quad \text{(imbibition)} \quad (5)$$

152

$$S_w^D(p_c, A_0, P_0) = \begin{cases} 1 & , p_c < p_D \quad (R_0 < r_D) \\ \frac{A_\Delta(p_c)}{A_0} & , p_c \geq p_D \quad (R_0 \geq r_D) \end{cases} \quad \text{(drainage)} \quad (6)$$

153

154 The total area  $A_\Delta$  of the triangular tube's water retaining corners,  $\gamma_{1,2,3}$  (i.e., the gray  
 155 areas in Figs. 4 and 5) is expressed by

$$A_\Delta(p_c) = \sum_{i=1}^3 A_{\gamma_i}(p_c), \quad (7a)$$

156 where

$$A_{\gamma_i}(p_c) = \left( \frac{1}{\tan \frac{\gamma_i}{2}} - \frac{(\pi - \gamma_i)}{2} \right) r_{AM}^2(p_c), \quad 0 < \gamma_i < \pi \quad (7b)$$

157 is the area of the triangle's  $i$ th water-filled corner (Tuller and Or, 1999). Consequently, the  
 158 total effective area  $A_\Delta$  **which is** still occupied by water is equal to the difference between the  
 159 (reduced) triangular pore area  $\tilde{A}$  and the area  $\pi r_{AM}^2$  of its respective inscribing circle (see Fig.

160 | 3). Above ~~equations~~Equations 7a + b can be simplified to  $A_{\Delta} = (3\sqrt{3} - \pi) r_{AM}(p_c)$  ~~when-if~~  
161 | considering equilateral triangles, i.e.,  $\gamma_{1,2,3} = \frac{\pi}{3}$ . The radius  $r_{AM}(p_c)$  of the reduced triangle's  
162 | arc meniscus can be directly calculated from Eq. 1. Calculated pressure-dependent water and  
163 | gas distributions during imbibition and drainage for an equilateral and arbitrary triangular  
164 | capillary are shown in Figs. 4a and 5a. The corresponding water retention curves plotted in  
165 | Figs. 4b and 5b illustrate the resulting hysteresis behavior of the partially saturated system  
166 | and can be subdivided into three parts: at low capillary pressures, i.e.,  $p_c < p_I$ , where the pore  
167 | always remains fully water-saturated. For the interval  $p_I < p_c \leq p_D$ , where two separate  
168 | behaviors are observed: during imbibition, the water content gradually increases with  
169 | increasing capillary pressure, while during drainage the pore still remains fully saturated. For  
170 | pressure levels  $p_c \geq p_D$ , both drainage as well as imbibition exhibit the same gradual  
171 | decrease of water saturation.

172 | In the following section, analytical solutions for respective NMR responses that arise  
173 | from partially saturated arbitrary triangular tubes are derived and matched against numerical  
174 | simulations by means of the generalized differential NMR diffusion equations introduced by  
175 | Brownstein and Tarr, 1979.

## 177 | 2.2 NMR response for triangular capillaries

178 | ~~NMR relaxometry is commonly employed for petrophysical investigations of saturated~~  
179 | ~~porous rocks in well logging and laboratory studies. In this respect, the NMR method is a~~  
180 | ~~unique geophysical tool, which delivers direct information about the water content and allows~~  
181 | ~~to infer the pore size distribution in rock samples or the subsurface.~~ The measured NMR  
182 | relaxation signal  $M(t)$  is constituted by superposition of all signal-contributing pores in a rock  
183 | sample (e.g., Coates et al., 1999; Dunn et al., 2002):



$$\frac{M(t)}{M_0} = \frac{1}{V_0} \sum_i^N \left( v_i \times \left( 1 - e^{-t/T_{i,1}} \right) \right), \quad (8)$$

184 where  $M_0$  and  $V_0$  are the equilibrium magnetization and total volume of the pore system,  
 185 respectively. The saturated volume of the  $i$ th pore and its corresponding longitudinal  
 186 relaxation constant are given by  $v_i$  and  $T_{i,1}$ , respectively.

187 Following derivations of Brownstein and Tarr (1979), the inverse of the longitudinal  
 188 relaxation time  $T_1$  is linearly proportional to the surface-to-volume ratio of a pore according  
 189 to

$$T_1^{-1} = T_{1B}^{-1} + \rho_s \frac{S_a}{V}, \quad (9)$$

190 where  $T_{1B}$  is the bulk relaxation time of the free fluid and  $\rho_s$  is the surface relaxivity, a  
 191 measure of how quickly protons lose their magnetization due to magnetic interactions with  
 192 paramagnetic impurities and reduced correlation times at the fluid-solid interface, which can  
 193 be attributed to paramagnetic ions at mineral grain surfaces.  $V$  and  $S_a$  are the pore's volume  
 194 and active surface boundaries, respectively. In this context, an active boundary refers to an  
 195 interfacial area, i.e., the pore wall, where  $\rho_s > 0$  and, thus, enhanced NMR relaxation will  
 196 occur as the molecules diffuse at the pore walls. This model, however, is based on the general  
 197 assumption of a relaxation regime that is dominated by surface relaxation processes (*fast*  
 198 *diffusion*), i.e., the fluid molecules move sufficiently fast and thus explore all parts of the pore  
 199 volume several times with respect to the time scale ( $\sim T_1$ ) of the experiment.

200 Upon consideration of a long (triangular) capillary, its surface-to-volume-ratio equals its  
 201 perimeter-to-cross-section-ratio, i.e.,  $S/V = P/A$ . Consequently, Eq. 9 can be written as

$$T_1^{-1} = T_{1B}^{-1} + \rho_s \frac{P_0}{A_0}, \quad (10)$$

202 where  $P_0$  is the saturated tube's (active) perimeter and  $A_0$  its cross-sectional area for a circular  
 203 cross-section,  $\frac{P_0}{A_0} = \frac{2}{r_0}$ , with  $r_0$  being the capillary radius. Hence, the relaxation rate of a fully

204 saturated arbitrary triangular pore  $ABC$  can be expressed in terms of its shape factor  $G$  and  
 205 perimeter  $P_0$ :

$$T_1^{-1} = T_{1B}^{-1} + \frac{\rho_s}{G P_0} \left( = T_{1B}^{-1} + \rho_s \frac{L_{AB} + L_{BC} + L_{CA}}{L_{AB} L_{CA} \sin(\gamma_A)} \right) , \quad (11)$$

206 where  $L_{AB}$ ,  $L_{BC}$ , and  $L_{AC}$  are the lengths of a triangle's sides and  $\gamma_A$  is the angle at corner  $A$   
 207 (see Fig. 3). As illustrated in Fig. 6, the relaxation times of a fully saturated pore decrease  
 208 with decreasing pore shape factor  $G$  – and thus, decreasing hydraulic conductance – and  
 209 increasing pore perimeter  $P$ . By reducing one angle from  $60^\circ$  to  $0^\circ$  while fixing another at  
 210  $60^\circ$ , we increase  $P/A$  for a constant cross-sectional area  $A$ . In the special case of an  
 211 equilateral triangular capillary, i.e.,  $P_0/A_0 = \frac{12}{\sqrt{3} L_0}$ , Eq. 11 can be simplified to

$$T_1^{-1} = T_{1B}^{-1} + \rho_s \frac{12}{\sqrt{3} L_0} . \quad (12)$$

213 Now we consider the previously discussed water-air system of a partially saturated  
 214 equilateral triangular capillary. Here, the NMR signal will originate from the water retained  
 215 at the corners. Replacing  $A_0$  in Eq. 10 with an effective area  $A_\gamma$  or  $A_\Delta$  as derived by Eqs. (7a)  
 216 and b, respectively.  $A_\Delta$  reflects the actual pore fraction that contributes to the NMR signal,  
 217 i.e., the portion of the pore area  $A_0$  that still remains occupied by water.

218 Supposing the air-water interface to be a passive boundary with respect to NMR surface  
 219 relaxivity, i.e.,  $\rho_s = 0$ , the effective active boundary is exclusively controlled by the pore  
 220 wall segments ( $\rho_s > 0$ ) in contact with water (wetting phase) (Fig. 7). Thus, the active  
 221 perimeter of such a partially saturated triangular capillary is equal to its pressure-dependent  
 222 reduced triangle's perimeter,  $P'_\Delta(r^{1D}(p_c))$ , according to

$$P_\Delta = \sum_{i=1}^{N=3} P_{\gamma_i} , \quad (13)$$

223 with

$$P_{\gamma_i} = 2 \frac{r_{AM}(p_c)}{\tan \frac{\gamma_i}{2}}, \quad 0 < \gamma_i < \pi \quad (14)$$

224 being the perimeter of the  $i$ th water-filled corner. Consequently, the NMR relaxation rates  
 225 and NMR signal (amplitude) evolution during drainage and imbibition of a single equilateral  
 226 triangular capillary can be expressed by

227

$$T_{\Delta,1}^{-1} = \begin{cases} T_{1B}^{-1} + \rho_s \frac{P_0}{A_0} & , \quad S_w^{I,D} = 1 \\ T_{1B}^{-1} + \rho_s \frac{P_{\Delta}^{I,D}(p_c, A_0, P_0)}{A_{\Delta}^{I,D}(p_c, A_0, P_0)} & , \quad S_w^{I,D} < 1 \end{cases} \quad (15)$$

228 and

$$\frac{m(t)}{m_0} = S_w^{I,D}(p_c, A_0, P_0) \left( 1 - e^{\frac{-t}{T_{\Delta,1}}} \right), \quad (16)$$

229 respectively. ~~Illustrated in~~ Fig. 8 ~~is illustrates~~ the pressure-dependent water distribution inside  
 230 a single equilateral triangular capillary (with a side length of  $1 \mu\text{m}$ ) during drainage (a) and  
 231 ~~corresponding~~ evolution of longitudinal magnetization (b). As the water saturation is reduced  
 232 with increasing pressure, both NMR amplitudes and relaxation times (c) decrease. Note that  
 233 only a single characteristic relaxation time at each saturation degree is observed, since each  
 234 corner has the same  $P_{\gamma}/A_{\gamma}$ , and consequently the same  $T_1$  value.

235 In contrast, each water-filled corner of a partially saturated non-equilateral triangle, i.e.,  
 236  $\gamma_1 \neq \gamma_2 \neq \gamma_3$ , can have a different  $P_{\gamma}/A_{\gamma}$  ratio, and thus will show a different relaxation time  
 237 and amplitude. As a result, depending on its individual shape, even a single partially saturated  
 238 pore exhibits a multi-exponential NMR relaxation behavior based on Eq. (8) according to

$$\frac{m(t)}{m_0} = \frac{1}{A_0} \sum_{i=1}^{N=3} A_{\gamma_i}^{I,D} \left( 1 - e^{\frac{-t}{T_{\gamma_i,1}}} \right), \quad (17)$$

239 with  $T_{\gamma_{i,1}} = \frac{1}{T_{1B}} + \rho_s \frac{P_{\gamma_i}}{A_{\gamma_i}}$  and  $\frac{A_{\gamma_i}^{I,D}}{A_0}$  being the characteristic relaxation time and amplitude  
 240 contribution of the  $i$ th corner of the triangle, respectively. Figure 9 exemplifies such different  
 241 multi-exponential relaxation behavior for a pore with a right triangle geometry with angles of  
 242 ( $\gamma_1 = 30^\circ, \gamma_2 = 60^\circ, \gamma_3 = 90^\circ$ ) and the same cross-sectional area as the equilateral pores in  
 243 Fig. 8 (i.e.,  $\sim$  NMR porosity).

244 To test the analytical (fast diffusion) models for partially saturated triangular capillaries  
 245 derived above, the calculated longitudinal NMR relaxation times and amplitudes are  
 246 compared to solutions obtained from 2D numerical simulations of the general NMR diffusion  
 247 equation (Mohnke and Klitzsch, 2010):

$$\dot{m} = \left( D \nabla^2 - \frac{1}{T_B} \right) m, \quad (18)$$

248 with normalized initial values  $m(\mathbf{r}, t = 0) = \frac{M_0 = 1}{A}$  and boundary conditions

$$D \mathbf{n} \nabla m \Big|_P = \rho_s m \Big|_P, \quad (19)$$

249 where  $m$  is the magnetization density,  $D$  the diffusion coefficient of water,  $T_B$  the bulk  
 250 relaxation time,  $\rho_s$  the interface's surface relaxivity,  $\mathbf{n}$  the outward normal, and  $A$  and  $P$  the  
 251 pore's cross-sectional area and perimeter, respectively. To support demonstrate the  
 252 consistency of the introduced model with numerical results obtained by Mohnke and Klitzsch  
 253 (2010), The above equations were solved numerically using finite elements (~~Mohnke and~~  
 254 ~~Klitzsch, 2010~~) to simulate the respective NMR relaxation data of the studied triangular  
 255 geometries.

256 As shown in Fig. 10, analytically (+) calculated NMR relaxation data for drainage and  
 257 imbibition for an equilateral triangular pore are in a very good agreement ( $R^2 > 0.99$ ) with  
 258 data obtained from numerical simulations (o).

259 | The model was also ~~validated~~ matched against numerical simulations for pores with  
260 | arbitrary angles. Figure 11 illustrates 2D finite elements simulations using saturated pore  
261 | corners with angles  $\gamma_i$  ranging from  $5^\circ$  to  $175^\circ$  with equal active surface-to-volume ratios  
262 |  $P_{\gamma_i}/A_{\gamma_i} = \text{const.}$  and thus  $T_{1,i} = \text{const.}$  The simulations were compiled and compared to  
263 | their respective analytical solutions. The ratios of the numerical to the analytical model  
264 | results for NMR amplitudes, i.e., NMR signal amplitudes,  $A_\gamma$ , and relaxation times,  $T_{1,\gamma}$  as  
265 | function of corner aperture  $\gamma$  are shown and confirm a near perfect correlation of  $R^2 > 0.99$ ,  
266 | with deviations generally less than 0.05 %. In this regard, the slight increase in divergence of  
267 | relaxation time ratios at acute and obtuse angles can be attributed to numerical errors  
268 | resulting from a decrease of the finite element's grid quality due to extremely high or low x-  
269 | to-y ratios at these apertures. ~~Note that the~~ The above model is applicable to any angular  
270 | capillary geometry, such as square or octahedron.

271

### 272 | **2.3 Simulated water retention curves and NMR relaxation data of partially saturated** 273 | **pore distributions**

274 | The goal of this section is to evaluate how pore shape affects the forward-modeled NMR  
275 | response of a partially saturated system of pores (a pore size distribution). As discussed  
276 | earlier, the NMR relaxation time of a single water-filled capillary pore is inversely  
277 | proportional to its surface-to-volume-ratio. Thus, at full water saturation, the relaxation-time  
278 | distribution obtained from a multi-exponential NMR relaxation signal represents the pore-  
279 | size distribution of the rock. At partial water saturation, it is often assumed that the NMR  
280 | relaxation signal still represents the pore size distribution of the water saturated pores (e.g.,  
281 | Stingaciu, 2010b), ~~which we~~ We are going to ~~show~~ demonstrate that this is valid is true for  
282 | ~~the~~ cylindrical but not for (tri-) angular pores.

283 In contrast to cylindrical pores, capillaries with (tri-)angular cross-sections may be partially  
284 water-saturated during drainage or imbibition (cf. Fig. 8 and 9) because of the water  
285 remaining in the corners. Thus, they show a different water retention behavior and the  
286 “desaturated” pores, i.e. their arc menisci, contribute to the NMR signal. Consequently, with  
287 increasing pressure (i.e. decreasing water saturation) the NMR relaxation behavior of the  
288 partially water-saturated triangular capillary pore bundle successively shifts to signal  
289 contributions with shorter relaxation times, exceeding the original distribution at full  
290 saturation. This shift reflects the fast relaxation of residual water trapped in the pore corners  
291 (Figure 12). This behavior in angular pore geometries is demonstrated in Figure 13. Here, the  
292 NMR relaxation components for a fully (blue line) and partially saturated (red and green)  
293 distribution of triangular capillaries are plotted. The green and red peaks show the signals of  
294 the residual water in the pore corners. ~~Following from As a consequence of the~~ reduced  
295 geometry concept the remaining water in the corners can be considered has the same similar  
296 in size and shape, i.e., due to the same NMR relaxation time, for all pores and thus only  
297 depends on pressure and not on pore size. independent on their size but dependent on  
298 pressure. Therefore with decreasing saturation, i.e., increasing pressure, the NMR signal of  
299 the arc menisci increases and shifts towards smaller relaxation times. If the non-wetting phase  
300 (air) has entered all capillaries, only one single relaxation time remains for the pore bundle of  
301 equilateral triangles. For arbitrarily shaped triangular pores, three relaxation times would  
302 remain for the de-saturated pore system. Hence, the concept of a relaxation time distribution  
303 assumed in conventional NMR inversion and interpretation approaches would be no longer  
304 valid.

305  
306 ~~All the same, we~~ We apply applied the concept of fitting multi-exponential relaxation time  
307 distributions to NMR transients calculated for pore bundles of circular and equilateral triangle

308 | cross-sections in order to study how pore shape affects the typically-shown relaxation time  
309 | distributions.

310 | Water drainage and imbibition with water as wetting and air as the non-wetting fluid were  
311 | investigated by simulating water retention curves and corresponding NMR relaxation signals  
312 | for a log-normal distributed pore size ensemble as shown in Figure 14.

313 | Herein, to clarify the subsequent discussion we focused only on the equilateral triangular  
314 | capillary model. ~~Note, that o~~Other angular pore shapes (e.g., right angular triangles or  
315 | squares) will exhibit a similar behavior. Capillary pressure curves presented in Figure 15a  
316 | were calculated from Eq. 1, 45, and 5-6 for pore bundles with circular and equilateral triangle  
317 | cross-sections. In contrast to water retention curves calculated for the cylindrical capillary  
318 | model significant hysteresis between drainage and imbibition can be observed for the  
319 | triangular capillary model, i.e. in terms of initial amplitudes (=saturation) and respective  
320 | mean relaxation times (Figure 15b). Corresponding NMR  $T_1$  ~~relaxation relaxation~~(saturation  
321 | recovery) signals shown in Figure 15c,d and e were calculated using a uniform surface  
322 | relaxivity of  $\rho_s = 10 \mu\text{m/s}$  and a water bulk relaxation  $T_{1,bulk} = 3 \text{ s}$ .

323 | The NMR  $T_1$  relaxation signals were simulated for 20 saturation levels of the drainage  
324 | and imbibition curves ranging from  $S = 100\%$  to  $S < 1\%$  water saturation. The corresponding  
325 | relaxation time distributions (Figure 15f-h) of the NMR  $T_1$  transients were determined by  
326 | means of a regularized multi-exponential fitting using a nonlinear least squares formulation  
327 | solved by the Levenberg-Marquardt approach (e.g., Marquardt, 1963; Mohnke, 2010).  
328 | Inverse modeling results of NMR data calculated for the drainage branches using the  
329 | cylindrical capillary bundle (Fig. 15f) exhibit a shift of the distribution's maximum towards  
330 | shorter relaxation times with decreasing saturation (i.e., increasing pressure). As anticipated,  
331 | the derived distribution functions remain inside the envelope of the relaxation-time  
332 | distribution curve at full saturation (see also Fig. 1a).

333 In contrast, inversion results for equilateral triangular capillary ensembles (Fig. 15f-h) –  
334 both for imbibition and drainage – show a similar shift to shorter relaxation times with  
335 decreasing saturation but also ~~move-shift towards the~~ outside the initial distribution at full  
336 saturation due to NMR signals originating from trapped water in the pore corners of the  
337 desaturated triangular capillaries. The effect of the pore corners on relaxation times at low  
338 saturations is also recognizable when comparing the (geometric) mean relaxation times,  
339 normalized ~~to-on~~ the values observed at full saturation (Fig. 15b): Both, the drainage and the  
340 imbibition hysteresis branch of the triangular pore bundle show smaller mean relaxation  
341 times than the cylindrical pore bundle.

342 In conclusion, the calculated inverse models for the triangular capillary bundle  
343 qualitatively agree with the behavior of the inverted NMR relaxation-time distributions at  
344 partial saturation that are frequently observed in experimental data, e.g., of the Rotliegend  
345 sandstone shown in Fig. 2.

### 346 **3 Summary and conclusions**

347 Experimental NMR relaxometry data and corresponding relaxation-time distributions  
348 obtained at partial water/air saturation were explicated by a modification of conventional  
349 NMR pore models using triangular cross-sections. ~~An-The derived~~ analytical solutions for  
350 calculating surface-dominated (fast diffusion) NMR relaxation signals in fully and partially  
351 saturated arbitrary angular capillaries ~~were introduced and validated consistent with~~  
352 ~~respective results obtained from~~ numerical simulations ~~of the general NMR diffusion~~  
353 ~~equations.~~

354 Shape and size of triangular pores ~~can~~ strongly influence both NMR ~~-amplitudes and~~  
355 ~~decay time distributions as well as and -the rock's~~ flow ~~properties, i.e., saturation and~~  
356 ~~(relative) permeability properties of rocks.~~ At full saturation ~~The-the~~ NMR relaxation time  
357 depends on the surface-to-volume ratio, which ~~again-in turn~~ depends on shape ~~when-if~~



358 considering angular pore capillaries. However, at partial saturation, the pore shape even more  
359 strongly influences the water distribution inside the pore system, and thus the NMR signal. In  
360 contrast to cylindrical capillaries, angular capillaries also contribute to the NMR signal even  
361 after desaturation of the pore due to the water remaining in the pore corners.

362 In this regard, non-equilateral triangular capillaries at partial saturation exhibit a three-  
363 exponential relaxation behavior due to different perimeter-to-surface (= surface-to-volume)  
364 ratios of the water in the pore corners whereas the relaxation time of the trapped water in the  
365 corners depends on pressure (~~but and~~ not on pore size). ~~Furthermore, the shape and size of the~~  
366 ~~triangular pores strongly influence both NMR and hydraulic properties. The NMR relaxation~~  
367 ~~time depends on the surface to volume ratio (and not on the pore shape), while In contrast~~  
368 ~~the water distribution inside the pore system, at partial saturation, is strongly influenced by~~  
369 ~~the shape of the pore. Thus~~ Therefore, it can be noted that the NMR signal at partial  
370 saturation is affected by ~~not only both~~ the surface-to-volume ratio, ~~but by~~ of the water  
371 saturated and the pore shape ~~of the desaturated pores as well~~.

372 Moreover, we studied the NMR response of a triangular pore bundle model by jointly  
373 simulating the water retention curves for drainage and imbibition and the corresponding  
374 NMR  $T_1$  relaxometry data. With decreasing water saturation, the simulated NMR relaxation  
375 distributions shift towards shorter relaxation times always below the initial distribution  
376 enveloped at full saturation, which is principally in agreement with the relaxation behavior  
377 observed in experimental NMR data from rocks (e.g., Figure 2b).

378 Ongoing research will include further experimental validation and implementation of the  
379 introduced approach in an inverse modeling algorithm for NMR data obtained ~~on~~ from  
380 partially saturated rocks to predict absolute and relative permeability at laboratory and  
381 borehole scales. Without considering angular pores the NMR signal of trapped water cannot  
382 be explained, i.e., using the classical approach of circular capillaries one cannot find a pore

383 size distribution which explains the relaxation time distributions at all saturations sufficiently  
384 (e.g., Mohnke, 2014). On the other hand, angular pore models can account for the trapped  
385 water and thus overcome the limitation of the classical approach. Moreover, following the  
386 approach of Mohnke (2014) but considering angular pores we strive for estimating surface  
387 relaxivity, pore size distribution, and pore shape by jointly inverting NMR data at different  
388 saturations. Based on the obtained pore size distribution and triangle shape we expect to  
389 improve the prediction of the absolute and relative permeabilities considerably.

390

### 391 **Acknowledgements**

392 The study was supported by the German Research Foundation (DFG) in the framework of  
393 the Transregional Collaborative Research Centre 32 (SFB TR 32) and Wintershall AG in the  
394 framework of Wintershall Tight Gas Consortium at RWTH Aachen University.

395

396 **References**

- 397 Al-Mahrooqi, S. H., Grattoni, C. A., Muggeridge A. H., Zimmermann, R. W., and Jing, X.  
398 D.: Pore-scale modelling of NMR relaxation for the characterization of wettability, J.  
399 Petrol. Sci. Eng., 52, 172–186, 2006.
- 400 Applied Reservoir Technology Ltd.: The NMR Sandstone Rock Catalogue, Long Melford,  
401 Suffolk, U.K., 1996.
- 402 Arnold, J., Clauser, C., Pechnig, R., Anferova, S., Anferov, V., and Blümich, B.: Porosity and  
403 Permeability from Mobile NMR Core-Scanning, *Petrophysics*, 47, 306–314, 2006.
- 404 Bird, N.R.A., Preston, A. R., Randall, E. W., Whalley, W.R. and Whitmore, A.P.:  
405 Measurement of the size-distribution of water-filled pores at different matric potentials by  
406 STRAFI-NMR relaxation-time measurements. *European Journal of Soil Science*. 56: 135-  
407 143, 2005.
- 408 Brownstein, K., and C. Tarr, C. (1979), Importance of classical diffusion in NMR studies of  
409 water in biological cells, *Phys. Rev. A*, 19, 2446–2453, 1979.
- 410 Chen, S., Liaw, H. K., and Watson, A. T.: Measurements and analysis of fluid saturation-  
411 dependent NMR relaxation and linebroadening in porous media, *Magn. Reson. Imaging*,  
412 12(2), 201–202, 1994.
- 413 Coates, G. R., Xiao, L., and, Prammer, M. G.: *NMR Logging Principles and Applications*,  
414 Halliburton Energy Services, Houston, TX, 234 pp., 1999.
- 415 Costabel, S.: Nuclear magnetic resonance on laboratory and field scale for estimating  
416 hydraulic parameters in the vadose zone, PhD thesis, Berlin University of Technology,  
417 2011. ([opus4.kobv.de/opus4-tuberlin/files/3173/costabel\\_stephan.pdf](http://opus4.kobv.de/opus4-tuberlin/files/3173/costabel_stephan.pdf))
- 418 Costabel, S. and Yaramanci, U.: Relative hydraulic conductivity in the vadose zone from  
419 magnetic resonance sounding - Brooks-Corey parameterization of the capillary fringe,  
420 *Geophysics*, 76(3), G61–G71, doi:10.1190/1.3552688, 2011.

421 Costabel, S. and Yaramanci, U.: Estimation of water retention parameters from nuclear  
422 magnetic resonance relaxation time distributions, *Water Resour. Res.*, 49(4), 2068–2079,  
423 doi:10.1002/wrcr.20207, 2013.

424 Desbois, G., Urai, J. L., Kukla, P. A., Konstanty, J., and Baerle, C.: High-resolution 3D fabric  
425 and porosity model in a tight gas sandstone reservoir: A new approach to investigate  
426 microstructures from mm- to nm-scale combining argon beam cross-sectioning and SEM  
427 imaging, *J. Petrol. Sci. Eng.*, 78, 243–257, doi:10.1016/j.petrol.2011.06.004, 2011.

428 Dong, M. and Chatzis, I.: The imbibition and flow of a wetting liquid along the corners of a  
429 square capillary tube, *J. Colloid Interface Sci.*, 172, 278–288, 1995.

430 Dunn K. J., Bergman D. J., and LaTorraca G. A.: Nuclear Magnetic Resonance:  
431 Petrophysical and Logging Applications, Pergamon: Elsevier Science, Amsterdam, 2002.

432 ~~Finjord, J., Hiorth, A., a Lad, U. H., and Skjaeveland, S. M.: NMR for equilateral triangular~~  
433 ~~geometry under conditions of surface relaxivity—analytical and random walk solution,~~  
434 ~~Transport Porous Med., 69, 33–53. arXiv:cond-mat/0508412v2, 2006.~~

435 Fleury, M., Deflandre F., and Godefroy, S.: Validity of permeability prediction from NMR  
436 measurements, *CR. Acad. Sci. Series IIC – Chemistry*, 4, 869–872, doi:10.1016/S1387-  
437 1609(01)01343-3, 2001.

438 Ioannidis, M., Chatzis, I., Lemaire, C., and Perunarkilli, R.: Unsaturated hydraulic  
439 conductivity from nuclear magnetic resonance measurements, *Water Resour. Res.*, 42(7),  
440 W07201, 6 pages, doi:10.1029/2006WR004955, 2006.

441 Jaeger, F., Bowe, S., van As, H., and Schaumann, G. E. (2009). Evaluation of  $^1\text{H}$  NMR  
442 relaxometry for the assessment of pore size distribution in soil samples. *European Journal of*  
443 *Soil Science*, 60:1052 – 1064.

444 Jia, P., Dong, M., and Dai, L.: Threshold pressure in arbitrary triangular tubes using RSG  
445 concept for all wetting conditions, *Colloid. Surface A*, 302, 88–95, 2007.

446 Kenyon, W.: Petrophysical principles of applications of NMR logging, Log Anal. 38(2), 21–  
447 43, 1997.

448 ~~Kleinberg, R.L.: Utility of NMR T2 distributions, connection with capillary pressure, clay  
449 effect, and determination of the surface relaxivity parameter  $\rho_2$ , Magn. Reson. Imaging,  
450 14(7), 761–767. doi: 10.1016/S0730-725X(96)00161-0, 1996.~~

451 Lenormand R., Zarcone C., Sarr, A.: A Mechanisms of the displacement of one fluid by  
452 another in a network of capillary ducts, J. Fluid Mech., 135, 337–353, 1983.

453 Liaw, H.-K., Kulkarni, R., Chen, S., and Watson, A.T.: Characterization of fluid distributions  
454 in porous media by NMR techniques, AIChE J., 42(2), 538–546, doi:  
455 10.1002/aic.690420223, 1996.

456 Marquardt, D. W.: An Algorithm for the Least-Squares Estimation of Nonlinear Parameters,  
457 Siam J. Appl. Math., 11(2), 431–441, 1963.

458 Mason, G. and Morrow, N. R.: Capillary behavior of a perfectly wetting liquid in irregular  
459 triangular tubes, J. Colloid. Interf. Sci., 141, 262–274, 1991.

460 Mayer, R. P., and Stowe, R. A.: Mercury porosimetry-breakthrough pressure for penetration  
461 between packed spheres, J. Colloid. Interf. Sci., 20, 893–911, 1965.

462 Mohnke, O.: Improved forward and inverse modelling of Surface NMR relaxation signals  
463 using multi-exponential decomposition, Ph.D. thesis, Technical University Berlin, Berlin,  
464 2010.

465 Mohnke, O. and Klitzsch, N.: Microscale Simulations of NMR Relaxation in Porous Media  
466 Considering Internal Field Gradients, Vadose Zone J., 9, 846–857,  
467 doi:10.2136/vzj2009.0161, 2010.

468 Øren, P. E., S. Bakke, and O. J. Arntzen, Extending predictive capabilities to network  
469 models, SPE Journal, 3, 324-336, 1998.

470 Or, D. and Tuller, M.: Flow in unsaturated fractured porous media: Hydraulic conductivity of  
471 rough surfaces. *Water Resour. Res.*, 36(5), 1165–1177, doi:10.1029/2000WR900020,  
472 2000.

473 Patzek, T. W., and D. B. Silin, Shape factor and hydraulic conductance in noncircular  
474 capillaries I. One-phase creeping flow, *Journal of Colloid and Interface Science*, 236,  
475 295-304, 2001.

476 Princen, H. M.: Capillary phenomena in assemblies of parallel cylinders I. Capillary rise  
477 between 2 cylinders, *J. Colloid. Interf. Sci.*, 30, 69–75, 1969a.

478 Princen, H. M.: Capillary phenomena in assemblies of parallel cylinders II. Capillary rise in  
479 systems with more than 2 cylinders, *J. Colloid. Interf. Sci.*, 30, 359–371, 1969b.

480 Princen, H. M.: Capillary phenomena in assemblies of parallel cylinders III. Liquid columns  
481 between horizontal parallel cylinders, *J. Colloid. Interf. Sci.*, 34, 171–184, 1970.

482 Ransohoff, T. C., and Radke, C. J.: Laminar flow of a wetting liquid along the corners of a  
483 predominantly gas-occupied noncircular pore, *J. Colloid Interface Sci.*, 121, 392–401,  
484 1987.

485 Seevers, D. O.: A nuclear magnetic method for determining the permeability of sandstones,  
486 *Society of Professional Well Log Analysts*, vol. 6, paper L, Houston, Texas, 1966.

487 Stingaciu, L. R.: Characterization of natural porous media by NMR and MRI techniques:  
488 High and low magnetic field studies for estimation of hydraulic properties, Ph.D. thesis,  
489 RWTH Aachen, URL: <http://darwin.bth.rwth-aachen.de/opus3/volltexte/2010/3392/>,  
490 2010a (accessed on 06/30/2014).

491 Stingaciu, L. R., Weihermüller, L., Haber-Pohlmeier, S., Stapf, S., Vereecken, H., and  
492 Pohlmeier, A.: Determination of pore size distribution and hydraulic properties using  
493 nuclear magnetic resonance relaxometry: A comparative study of laboratory methods.  
494 *Water Resour. Res.*, 46, 1–11, doi:10.1029/2009WR008686, 2010b.

495 Talabi, O., AlSayari, S. Iglauer, I., and Blunt, J.: Pore-scale simulation of NMR response, J.  
496 Petrol. Sci. Eng., 67, 168–178, 2009.

497 Thern, H.: Examining the fluid film model in porous media by NMR rock catalogue data,  
498 Symposium of the Society of Core Analysts, Avignon, France, paper SCA2014-051.

499 Tokunaga, T. K. and Wan, J.: Water film flow along fracture surfaces of porous rock, Water  
500 Resour. Res., 33(6), 1287–1295, doi:10.1029/97WR00473, 1997.

501 Toledo, P. G., Novy, R. A., Davis, H. T., and Scriven, L. E.: Hydraulic Conductivity of  
502 Porous Media at Low Water Content, Soil Sci. Soc. Am. J., 54, 673–679,  
503 10.2136/sssaj1990.03615995005400030007x, 1990.

504 Torrey, H. C.: Bloch equations with diffusion terms, Phys. Rev., 104(3), 563–565,  
505 doi:10.1103/PhysRev.104.563, 1956.

506 Tuller, M., Or, D., and Dudley, L.M.: Adsorption and capillary condensation in porous media  
507 - liquid retention and interfacial configurations in angular pores, Water Resour. Res.,  
508 35(7), 1949–1964, doi: 10.1029/1999WR900098, 1999.

509 Tuller, M. and Or, D.: Hydraulic conductivity of variably saturated porous media: Film and  
510 corner flow in angular pore space, Water Resour. Res., 37(5), 1257–1276, DOI:  
511 10.1029/2000WR900328, 2001.

512      FIGURES

513



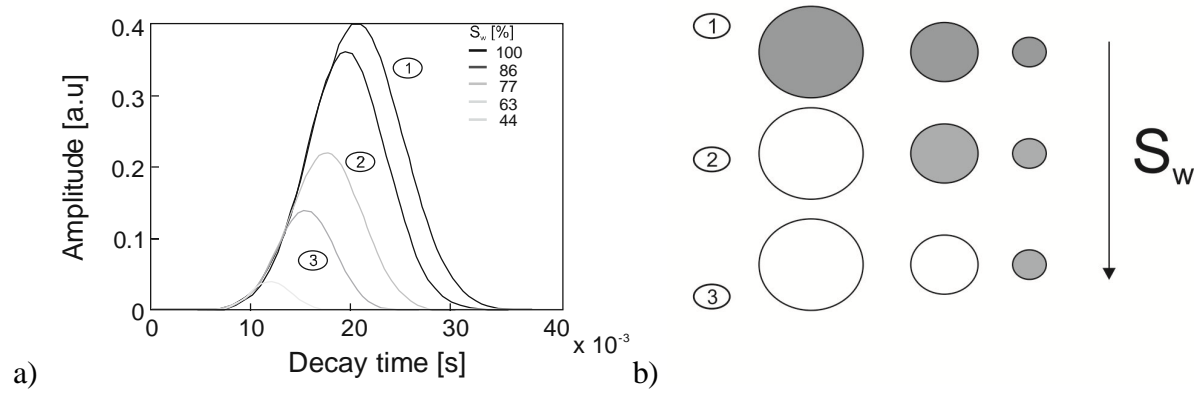


**Figure 1.** a) NMR decay time distributions at different water saturation levels for a classical cylindrical capillary pore distribution. b) Concept sketch of saturated (gray) and de-saturated capillaries, e.g., during drainage.

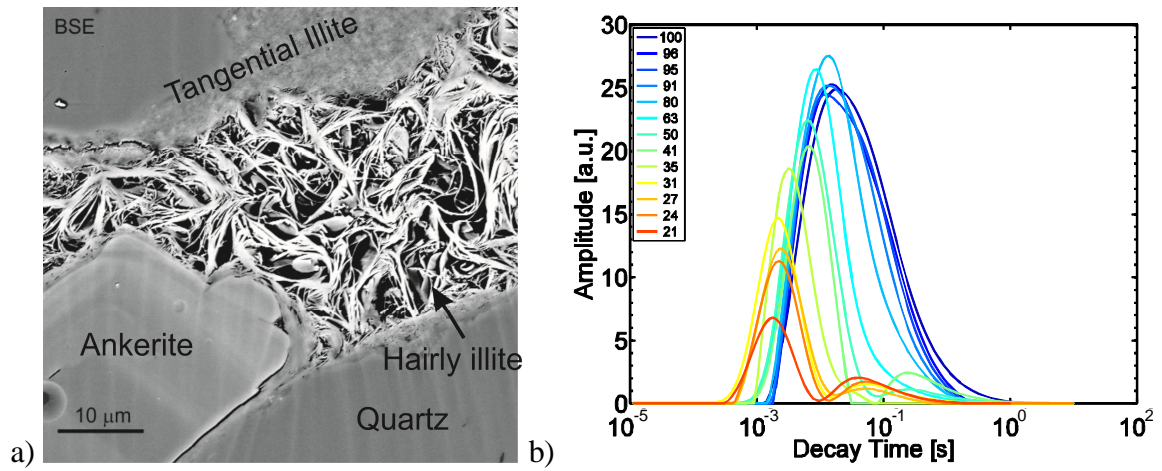
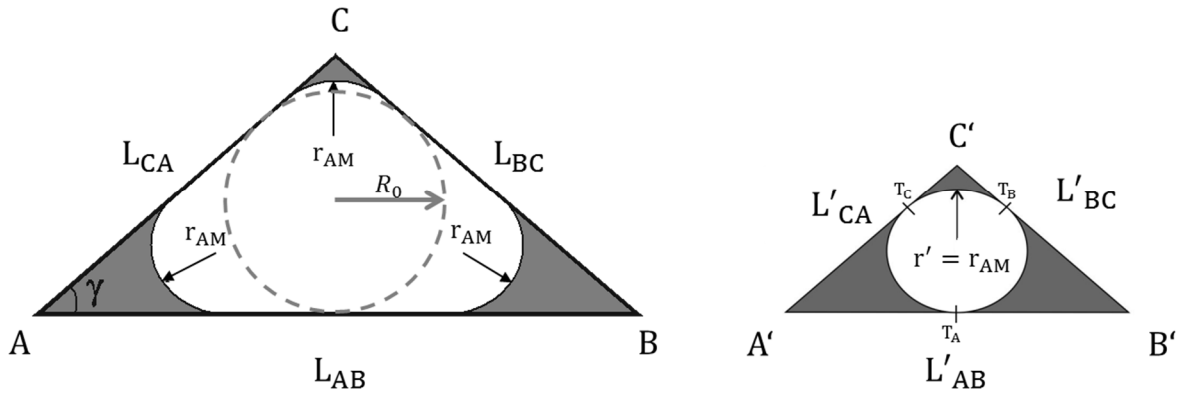


**Figure 2.** a) Complex pore structure of a Rotliegend tight gas sandstone. Pore spaces are filled with tangential and hairy illite and exhibit different pore types with elongated or slit-shaped, triangular, and multi-angular cross-sections. b)  $T_1$  decay time distributions calculated from inverse Laplace transform performed on Rotliegend sandstone (porosity 13%, permeability 0.1 mD) at different water saturations ( $S_w = 21\% - 100\%$ ).



a)

b)

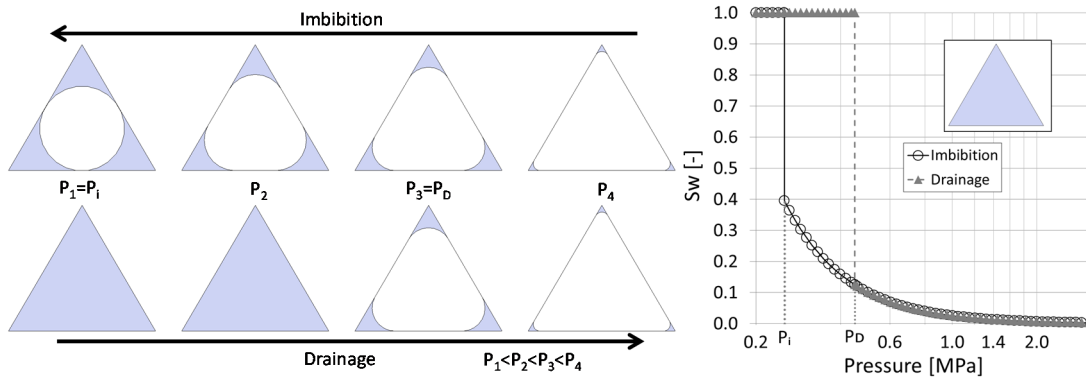
**Figure 3.** Cross-sections of a partially saturated triangular tube. Arc meniscus of radius  $r_{AM}$  separates invading non-wetting phase (white) from adsorbed wetting phase (gray). a)

Original triangle  $ABC$  with side lengths  $L_{AB}, L_{BC}, L_{CA}$ , and radius  $R_0$  of its inscribing circle.

b) Reduced triangle  $A'B'C'$  of similar geometry. The wetting phase resides in the three corners (gray) with  $r' = r_{AM}$  being the radius of both the three interface arc menisci of  $ABC$  and of the inscribing circle of  $A'B'C'$

516

517



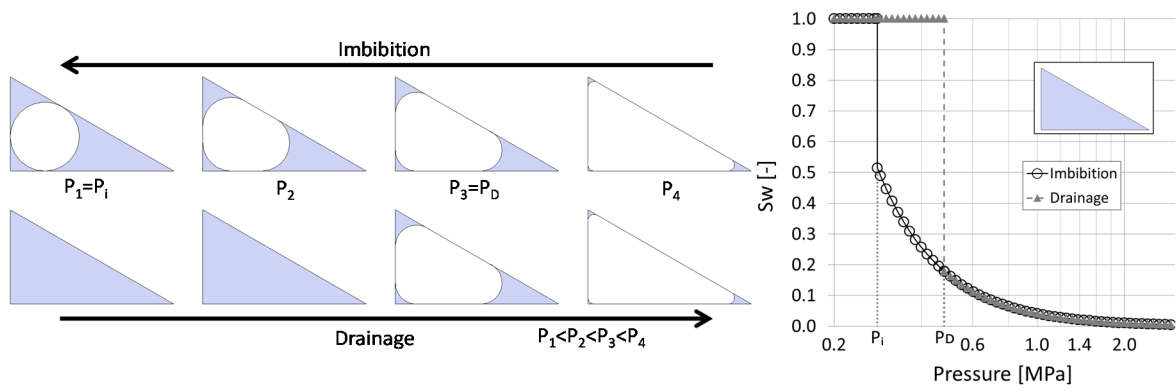
a)

b)

**Figure 4.** a) Modeled distribution of water (gray) and gas (white) phases in an equilateral triangular tube with a side length of  $1 \mu\text{m}$  during imbibition (top) and drainage (bottom). b) Water saturation versus capillary pressure during imbibition ( $\circ$ ) and drainage ( $\blacktriangle$ ).

518

519



a)

b)

**Figure 5.** a) Modeled distribution of water (gray) and gas (white) phases in a right-angled triangular capillary ( $G = 0.39$ ) with side lengths  $L = 1, 0.81, 0.58 \mu\text{m}$ , and perimeter  $P = 2.39 \mu\text{m}$  during imbibition (top) and drainage (bottom). b) Water saturation versus capillary pressure during imbibition ( $\circ$ ) and drainage ( $\blacktriangle$ ).

520

521

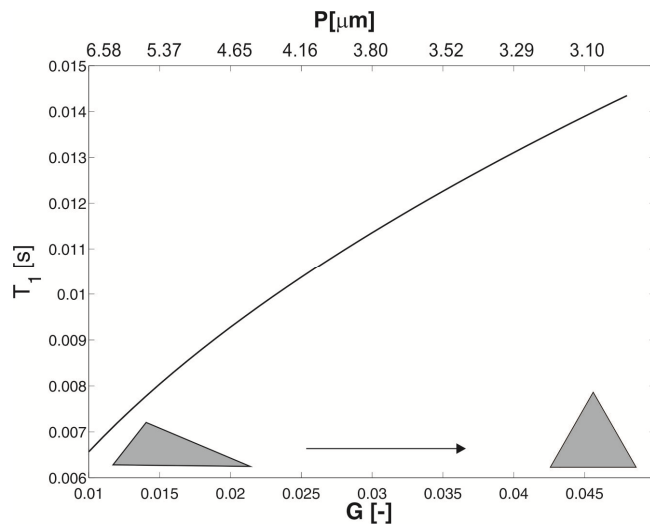


**Figure 6.** Longitudinal relaxation times  $T_1$  of fully saturated triangular pores with constant cross-sectional area  $A = 4.33 \cdot 10^{-13} \text{ m}^2$  versus shape factor  $G = \frac{A}{P^2}$  and perimeter  $P$ . NMR

parameters:  $\rho_s = 10 \mu\text{m}/\text{ss}^{-1}$ ,  $T_{1B} = 3 \text{ s}$ .

522

523

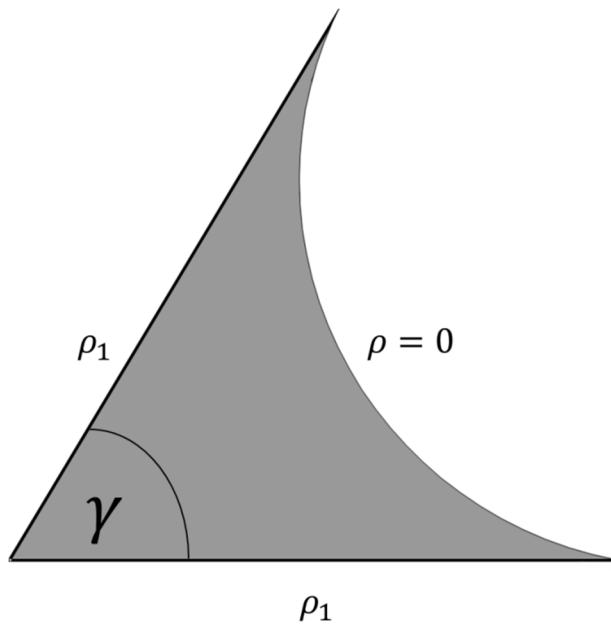


**Figure 7.** Saturated corner with active boundaries, i.e.,  $\rho_s = \rho_1 > 0$  at the corner's perimeter  $P_\gamma$  and a passive boundary at the air-water interface (meniscus), i.e.,  $\rho_s = \rho = 0$ .

524

525

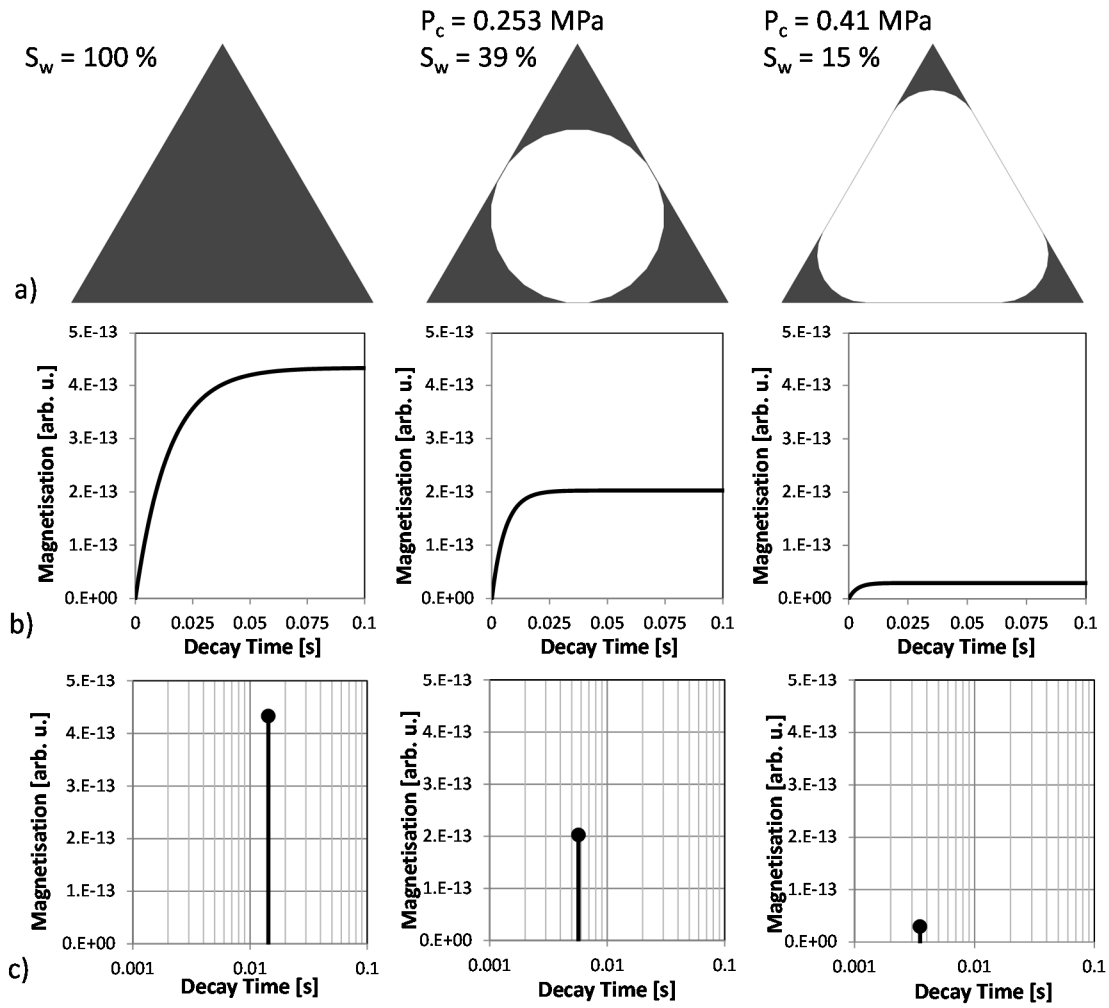


**Figure 8.** Water (black) and air (white) distributions within a triangular pore ( $A_0 = 4.33 \cdot 10^{-13} \text{ m}^2$ ,  $\rho_s = 10^{-5} 10 \mu\text{m/s}$ ) at different capillary pressures for imbibition (a) with corresponding evolution of the (longitudinal) magnetization (b) and NMR  $T_1$  relaxation times (c).



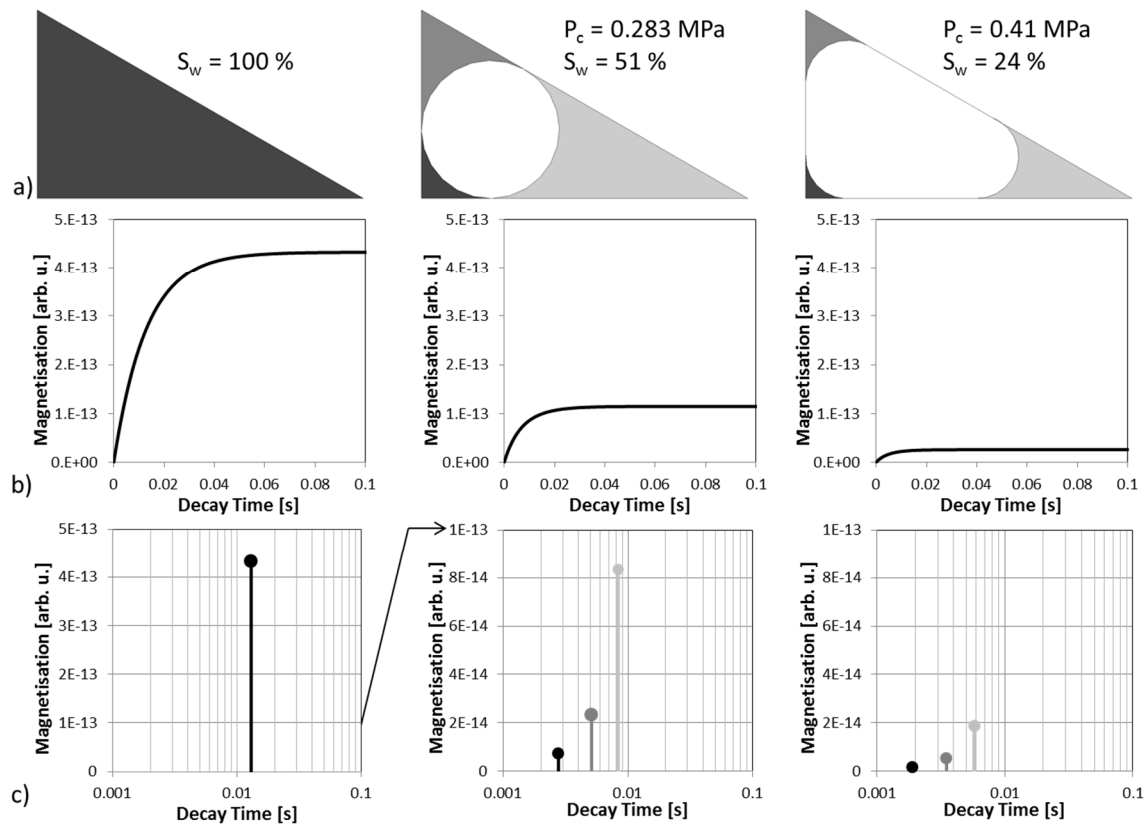
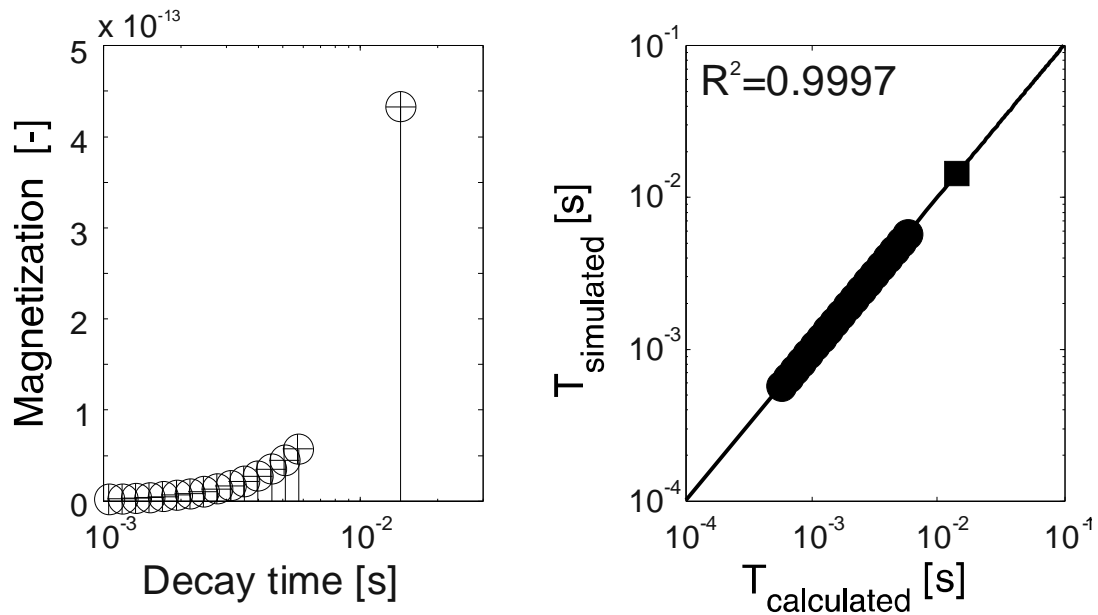


**Figure 9.** Water (black and grays) and air (white) distributions within a right-angled triangular pore ( $A_0 = 4.33 \cdot 10^{-13} \text{ m}^2$ ,  $\rho_s = 10 \text{ } \mu\text{m s}^{-1}$ ) at different capillary pressures for imbibition (a) with corresponding evolution of the (longitudinal) magnetization (b) and NMR  $T_1$  relaxation times (c).

528

529



a)

b)

**Figure 10.** NMR response of an equilateral triangular capillary pore model (with a side length of  $1 \mu\text{m}$ ). a) Magnetization versus  $T_1$  decay time data of numerical ( $\circ$ ) and analytical solutions ( $+$ ) for all applied pressure levels. b) Cross-plot of numerically simulated and analytically calculated longitudinal  $T_1$  decay times at partial ( $\bullet$ ) and full water saturation ( $\blacksquare$ ). A corresponding water saturation versus capillary pressure diagram is shown in Fig. 4.

530

531

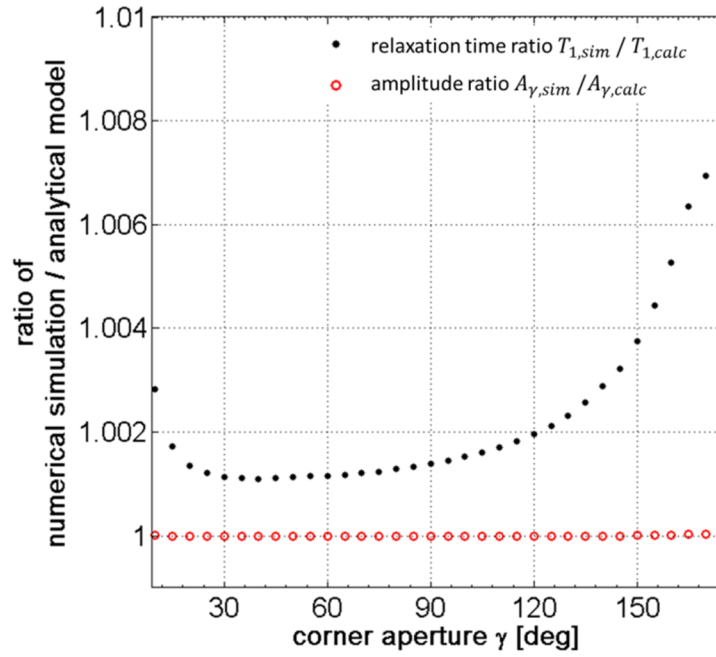


**Figure 11.** Comparison of analytical and calculated NMR relaxometry data originating from

saturated pore corners (e.g. see Fig. 7) of varying apertures ( $5^\circ < \gamma < 175^\circ$ ) and equal

active surface-to-volume ratio  $\frac{P_{\gamma i}}{A_{\gamma i}} = const.$  (NMR model parameters;  $T_{1B} = 3s$ ,

$D = 2.5 \cdot 10^{-9} \text{ m}^2 \text{ s}^{-1}$ ,  $\rho_s = 10 \mu\text{m s}^{-1}$ ).

532

533

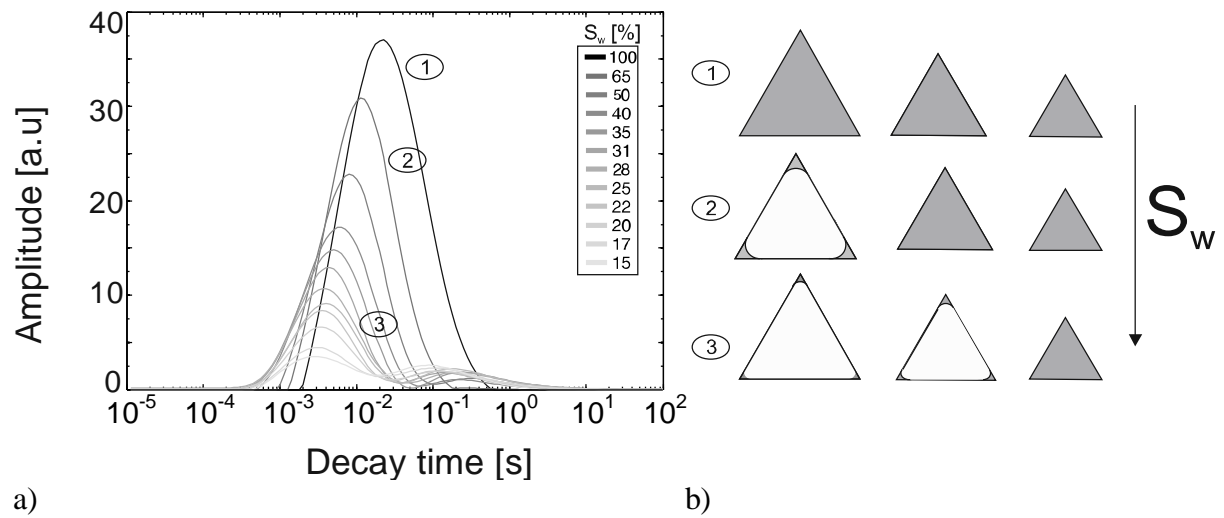


**Figure 12.** a) NMR decay time distributions at different water saturation levels for a pore distribution of equilateral triangles. b) Concept sketch of saturated (gray) and de-saturated triangular capillaries for increasing pressure levels (1), (2) and (3), e.g., during drainage.

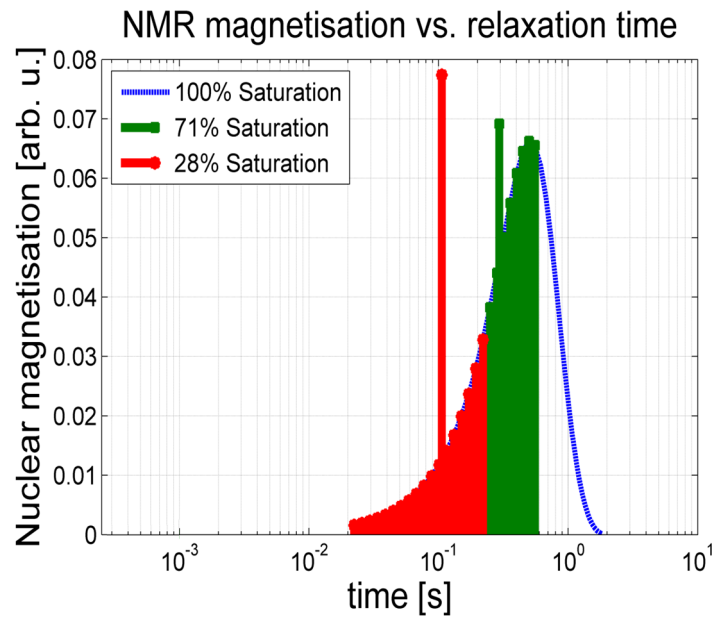


Figure 13: Relaxation components of fully (blue line) and partially de-saturated triangular pore size distribution. At a specific saturation level all pore corners with residual saturation exhibit the same NMR magnetization and relaxation behavior, thus superposing to a single fast relaxation component (e.g. red and green bars)

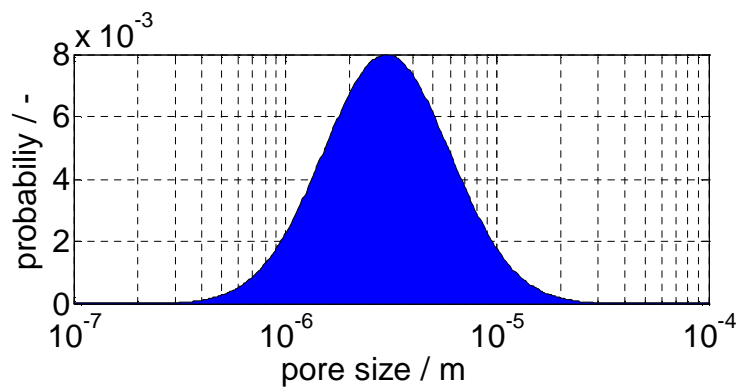


Figure 14. Pore-size distribution model (log-normal distribution:  $\sigma = 0.3$ ,  $\mu = 3 \cdot 10^{-6} \text{ m}$ ) in analogy to that of the Rotliegend Sandstone shown in Fig. 2.

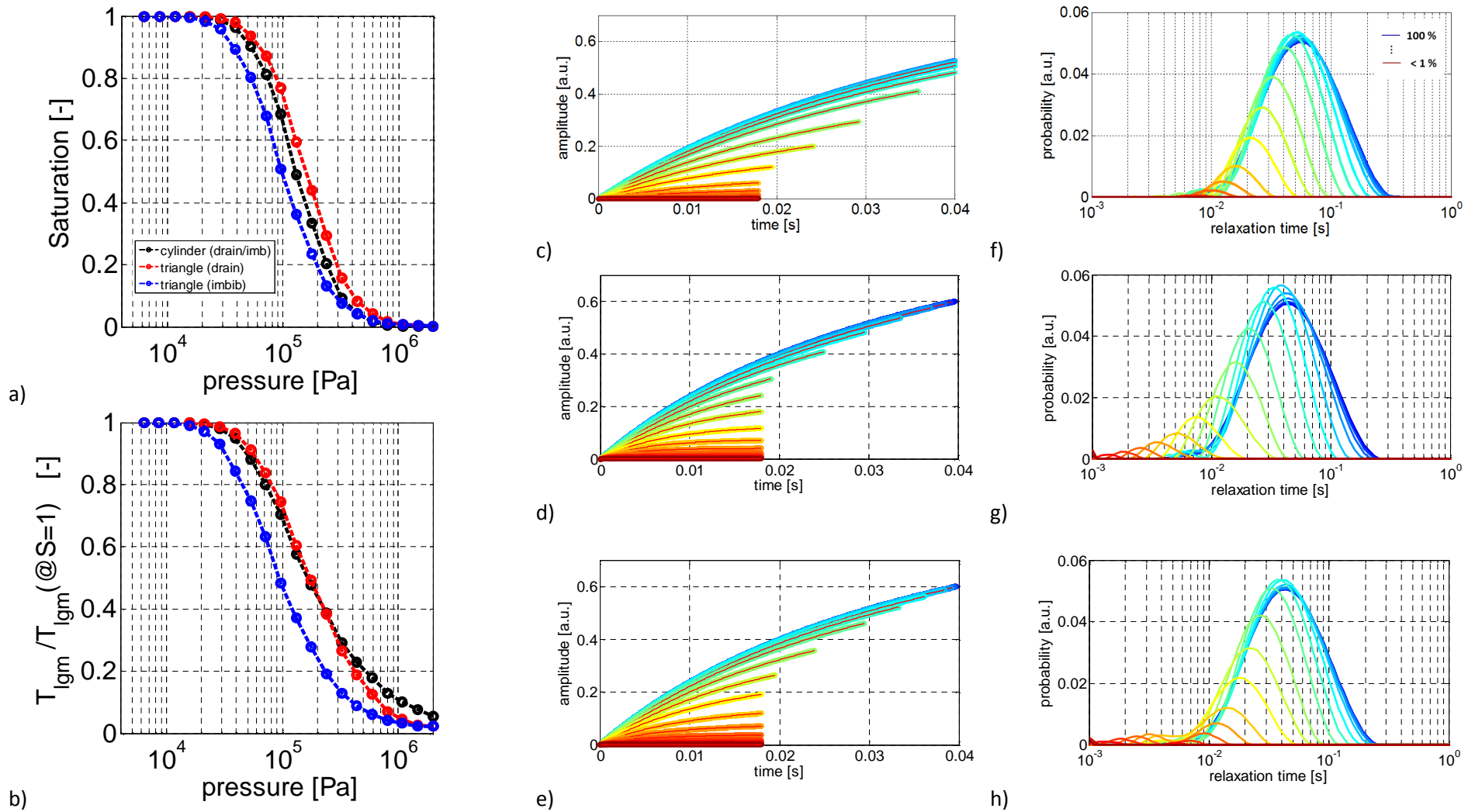


Figure 15: a) Modeled drainage and imbibition curves for circular and equilateral triangular capillary ensemble (cf Figure 14) and b) Corresponding normalized mean NMR  $T_1$  relaxation times vs pressure curves. Modeled and fitted (red lines) NMR transient signals (longitudinal magnetization evolution) corresponding inverted NMR  $T_1$  relaxation time distributions for 20 fully and partially saturated pore-size distributions ranging from < 1 % to 100 % saturation using circular (c, f) and equilateral triangular capillaries during imbibition (d, g) and drainage (e, h).

